Design and Performance of A High Resolution μ-Spec: An Integrated Sub-millimeter Spectrometer

Emily M. Barrentine[a], Giuseppe Cataldo[a,b], Ari D. Brown[a], Negar Ehsan[a], Omid Noroozian[a,c], Thomas R. Stevenson[a], Kongpop U-Yen[a], Edward J. Wollack[a], and S. Harvey Moseley[a]

[a]NASA Goddard Space Flight Center, Greenbelt, MD, USA
[b]Universities Space Research Association, Columbia, MD, USA
[c]University of Maryland-College Park, College Park, MD, USA

ABSTRACT

μ-Spec is a compact submillimeter (~ 100 GHz-1.1 THz) spectrometer which uses low loss superconducting microstrip transmission lines and a single-crystal silicon dielectric to integrate all of the components of a diffraction grating spectrometer onto a single chip. We have already successfully evaluated the performance of a prototype μ-Spec, with spectral resolving power, R=64. Here we present our progress towards developing a higher resolution μ-Spec, which would enable the first science returns in a balloon flight version of this instrument. We describe modifications to the design in scaling from a R=64 to a R=256 instrument, as well as the ultimate performance limits and design concerns when scaling this instrument to higher resolutions.

Keywords: Far-infrared, submillimeter, spectrometer, superconducting transmission line, Kinetic Inductance Detectors

1. INTRODUCTION

Submillimeter spectroscopy from a space- or balloon-borne instrument will enable the study of heavily obscured IR luminous galaxies at high redshifts, allowing us to form a clearer picture of the evolution of structure and star formation in our universe across cosmic time. A submillimeter survey could not only do the same sort of tomography of the epoch of initial galaxy formation that is anticipated with 21 cm surveys, but could simultaneously trace the evolution of physical conditions of the interstellar medium in both normal and star-forming galaxies. The brightest fine structure lines of abundant elements (C, N, and O) in star-forming galaxies are seen in the $50-200$ μm rest frame. A spectrometer operating from $420-800$ μm could observe these lines in ultraluminous star-forming galaxies over redshifts from $z \sim 2-6$.[1]

Current submillimeter spectrometers deployed on ground-based instruments, for example Z-spec,[2] are unable to meet the requirements of a space-borne instrument due to size, weight and power constraints. However, arrays of hundreds of integrated spectrometers, like μ-Spec, with sensitive detectors, on a cryogenic (4K) telescope in space, such as an an instrument on the Far-Infrared Surveyor being considered in the next Decadel Survey,[3] could transform the capability of such a space mission.

We have designed, fabricated, and demonstrated a laboratory μ-Spec instrument with resolving power, $R = \lambda/\Delta\lambda = 64$.[4–6] Here we first present an overview of the μ-Spec instrument and its components. We then discuss the ultimate performance limits of the instrument, and comment on some of the specific modifications required in moving from the lower resolution $R = 64$ design to higher resolutions. Finally, we present our design for a $R = 256$ spectrometer targeted for a balloon-borne science instrument.

Further author information: (Send correspondence to E.M.B.)
E.M.B.: E-mail: emily.m.barrentine@nasa.gov, Telephone: 1 301 286 9501

2. DESIGN OVERVIEW

μ-Spec works as an analog to a diffraction grating spectrometer, in which the light is split and a linear phase gradient is introduced, with the resulting wavefronts interfering to come into focus at spatially separated locations on a focal plane, dependent upon their wavelength. μ-Spec integrates all of the elements of a diffraction grating spectrometer onto a single silicon wafer in photolithographically patterned superconducting transmission line. The components are implemented in a low-loss single crystal silicon dielectric to achieve high efficiency (see Sec. 3.4).
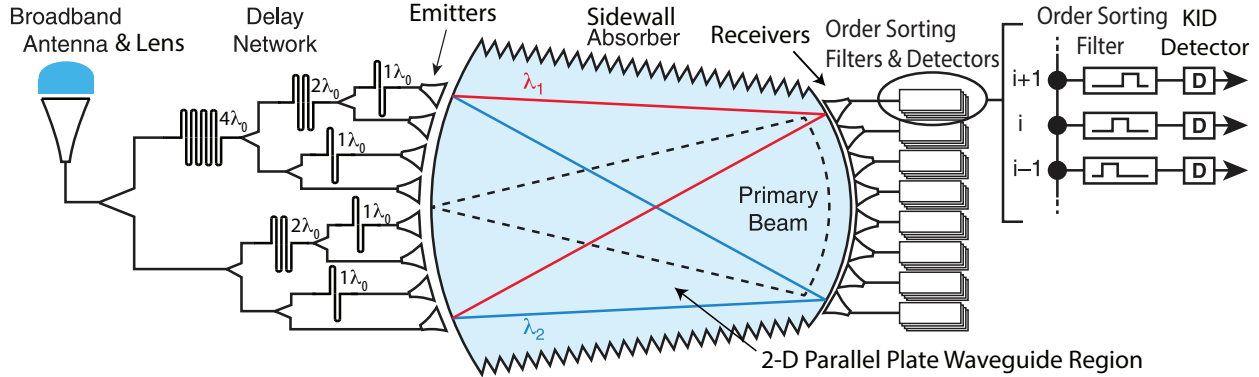

Figure 1. A cartoon of the μ-Spec instrument showing the individual instrument components. All of these components are integrated on a silicon chip using superconducting planar transmission line. Modified from Ref. 5.

In the μ-Spec instrument a broadband slot antenna (see Fig. 1) provides efficient submillimeter wave coupling from free space over the entire spectrometer bandwidth. A hyper-hemispherical silicon lens mounted directly to the back of the silicon chip is used to increase the beam directivity, and an anti-reflective coating technique can be applied to the lens to improve optical efficiency.[7] This slot antenna transitions to superconducting microstrip transmission line where the submillimeter light is split into N equal beams in a 'delay network' where a linear phase delay gradient across the pupil is introduced. The maximum delay length required is set by the resolution of the instrument and the operating wavelength, such that the additional delay length in the longest path of the delay network is equal to $R\lambda$. The high refractive index of the silicon allows the large phase delays for a high resolution spectrometer to occupy a compact area on a silicon wafer. The resolving power of the instrument is similarly related to N by $R = NM$ where M is the order of operation, as defined in the analog of the spectrometer grating equation.[8]

An emitter feed is used to transition from these microstrip lines and to launch the submillimeter signals into a 2-D parallel plate waveguide region. In this region the circular wavefronts interfere and come into focus at locations on a focal plane, separated by wavelength. A meta-material absorbing structure, consisting of arrays of circular resistors overlaying the top edges of the 2-D waveguide in the sidewall regions, absorb any reflected signals or unused orders, preventing confusion due to scattered light.

The focal plane architecture is in a Rowland configuration, where the focal plane radius is the Rowland circle radius. This same design, used in the microwave region, is called an Archer lens.[9,10] The imaging along the focal surface can be optimized to produce diffraction-limited images using the procedures described by Ref. 11 for Z-Spec. Details of the μ-Spec focal plane design methodology can be found in Refs. 5,8. Receiving feed channels at these focal plane locations transition again to microstrip transmission line and then to Kinetic Inductance Detectors (KIDs)[12,13] where the signal is detected. KIDs are intrinsically frequency multiplexed and can be simultaneously observed and readout by a single microwave line using standard digital radio techniques.[14,15] In μ-Spec designs operated in higher order (see Sec. 4.1) broadband order-sorting filters send the different orders to separate KID detectors.

We choose to implement microstrips planar transmission lines (rather than co-planer waveguide transmission lines) for both our submillimeter transmission lines and KIDs to provide good immunity to stray light, and very

low KID-to-KID crosstalk. In addition, loss above the superconducting gap prevents unwanted coupling to the transmission lines. Furthermore, selected regions of the spectrometer chip are patterned with a thin film absorber (~ 100 Ohms/sq) to terminate stray radiation. As another line of defense, an absorbing enclosure resides beyond the package and the microwave readout feedlines are protected via thermal blocking filters.[16,17]

It should be noted that many of the components of the μ-Spec instrument are required for any integrated instrument of this kind (for example, other integrated submillimeter spectrometers under development, such as Super-Spec[18,19] and DESHIMA[20,21]). These common components include highly efficient but controlled optical coupling to the sky, low-loss superconducting transmission lines, KID detectors and microwave readout. However, the delay network, 2-D parallel plate waveguide region, focal plane and emitter and receivers are unique components necessary for the diffraction grating analog design. This diffraction grating analog design provides intrinsically high efficiency and is relatively insensitive to lithographic errors and other fabrication variations and material loss (see Sec. 3.4 and 3.3). The diffraction grating analog design also provides the capability for uniform Nyquist sampling of the spectrum and high spectral purity (see Sec. 3.1).

3. EXPECTED PERFORMANCE

3.1 Sampling Capability & Spectral Purity

The spectral function of the instrument closely follows the $sinc^2$ function, $[sin(x)/x]^2$, the Fourier transform of the uniformly illuminated synthetic grating, providing excellent spectral purity. This is illustrated in Fig. 6 for the specific case of our $R = 256$ design. For the diffraction grating analog design the absolute frequency for each channel is also determined by the submillimeter design and is insensitive to fabrication tolerances. Thus, the sampling of the spectrum can be made uniform and precise. The Nyquist sampling requirement requires that the spectral function be sampled twice for each full width at half maximum (FWHM) spacing. With the submillimeter receiver designs that we have explored for both the $R = 64$ and 256 design it is possible to achieve this Nyquist sampling criterion, while also achieving high efficiency. For efficient Nyquist sampling and flexibility in beam width, however, a phased array may be a more versatile feed design. Thus, we are presently investigating a new magnetically-coupled radiator design for the receiver component which naturally provides better impedance matching to the parallel plate waveguide region, and decouples the impedance-matching constraint from the ability to adequately sample the focal plane. This design is analogous to the slot antenna design[32] which is used in BICEP II, MUSIC, and MAKO instruments.

3.2 Frequency Coverage

The lowest operating frequency for the instrument is limited by the gap frequency of the KID detector material. In both the $R = 64$ and $R = 256$ versions of this instrument we use thin film aluminum for our KID absorber material, with $f_{gap} \sim 110$ GHz. The highest operating frequency is limited by the gap energy of the superconducting transmission line material. In both the $R = 64$ and $R = 256$ versions we use thin film niobium, with $f_{gap} \sim 675$ GHz. In future versions of this instrument we intend to employ niobium-titanium nitride films for the superconducting transmission line material, which will allow us to extend the operating frequency up to ~ 1.1 THz.

Our planned $R = 256$ design will operate between $350 - 650$ GHz (see Sec. 5) well within the limits set by our materials and near the limits of our current submillimeter design. We are presently investigating what limits our submillimeter design choices place on the frequency bandwidth of a single μ-Spec instrument. The components of the instrument which impact the bandwidth include: 1) A limitation to achieving high receiver coupling efficiency and an increase in confusion due to reflected beams, when extending the receivers to high angles around the focal plane in order to extend the frequency bandwidth; 2) Stop bands that arise in the delay network due to slight reflections from the bends in the meandered lines. 3) Bandwidth limitations corresponding to chosen designs for the slot-antenna, power splitters (in the phase delay network), emitters and receivers. We briefly discuss the first two of these design issues here.

In our current delay network design (used in our $R = 64$ design) the spacing between bends is periodic. Unwanted reflections at the bends (≤ 20 dB) are concentrated in narrow stop bands where transmission is reduced as is shown in Fig 2, and where phase error may also be introduced. As the delay network is scaled up to

larger sizes for higher resolution designs, we expect the width of the stop bands to tend to grow narrower. In our present design scheme we can simulate, predict and adjust the locations of these stopbands by adjusting the bend spacings in order to bracket the spectrometer band. This method allows us around an octave of bandwidth. One method to increase this bandwidth is to increase the bend radius to reduce the level of reflected signal. A second scheme is to make the bend spacings random or unperiodic in order to spread these reflections out across the spectrometer band. However, the effect of such a scheme on spectrometer performance needs to be investigated further.
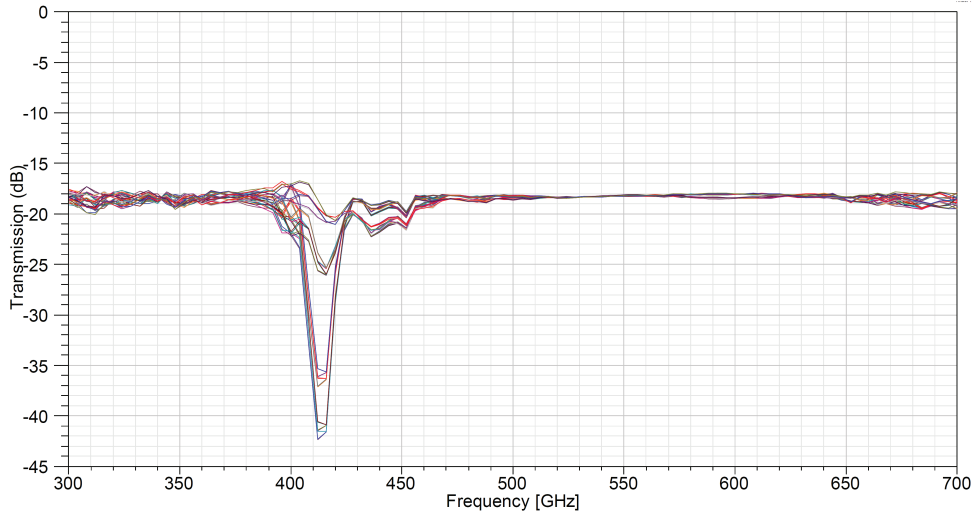
Simulated transmission from input to port N

Figure 2. HFSS simulation of the $R = 64$ delay network transmission between the delay network input port to each of the 64 output ports, showing a stop band due to reflections off of the periodic bends (microstrip width = bend radius= 10.5 μm) in the delay network. It should be noted that the limitation of the bandwidth of our current power splitter design is also seen in these simulation results. In our current design scheme we adjust the periodic spacing between bends to adjust the stopband locations to bracket the spectrometer band. As the delay network is scaled up from $R = 64$ to higher resolutions, we expect the width of the stop bands to become narrower.

In order to ensure full simultaneous coverage when operating in higher orders, and to maximize the bandwidth, the focal plane sampling should be extended towards higher angles. We are also presently exploring what the limits are to extending this sampling to high angles. At high angles around the focal plane one becomes limited by both the receiver efficiency and confusion effects from reflections. At such a point, one option may be to increase the focal plane radius (at the cost of a larger size instrument) to reduce the angle required for a given frequency bandwidth.

3.3 Phase Error

The focal plane design can be optimized following the procedures described in Refs. [5, 8] to achieve phase error that is significantly below our design criterion of $2\pi/14$, a typical value taken for diffraction limited imaging systems. This is illustrated for our $R = 256$ design in Fig. [5]. Likewise, there is no significant phase error due to fabrication tolerances that introduce random variations along the phase-sensitive transmission lines in the spectrometer. We measure variations in niobium width of less than ≤ 0.2 μm across a four-inch wafer in our niobium films fabricated using a novel metallic thin film liftoff technique,[22, 23] which also maintains the integrity of the silicon surface. Our niobium film thickness tolerances do not limit the phase delay since our films are several times the superconducting penetration depth. We use single crystal silicon for our dielectric which eliminates variations in dielectric constant. To do so we use a novel void-free low temperature wafer-scale bonding technique which maintains pristine integrity of the Si dielectric.[22] We measure thickness variations ≤ 25 nm in 450 nm thick silicon device layers in silicon-on-insulator (SOI) wafers purchased from SOITEC and made

4

using the Smart-Cut process.[24] From these measured tolerances we can calculate the phase error as a function of the instrument resolution along our transmission line paths for each of the phase-sensitive regions, including the delay network, the interconnect between the delay network and the emitter array, and the 2-D parallel plate waveguide region. In this calculation we take into account how the area of each of these elements scales with resolving power. We assume that the instrument operates in higher orders and that the Rowland circle radius and 2-D parallel plate waveguide extent remain constant in size as we move to higher resolutions. We also consider how the measured profile on the wafer of these fabrication variations corresponds to the orientation of the physical layout of the instrument elements. This analysis indicates that as we scale towards high resolutions the phase error is dominated by the error introduced in the delay network portion of the instrument. Our analysis also indicates that we can scale to $R \geq 2300$ and still remain below our phase error criterion of $\leq 2\pi/14$. We expect then to be ultimately limited in resolution not by fabrication tolerances, or by submillimeter design constraints, but by material loss, as is described in the following section.

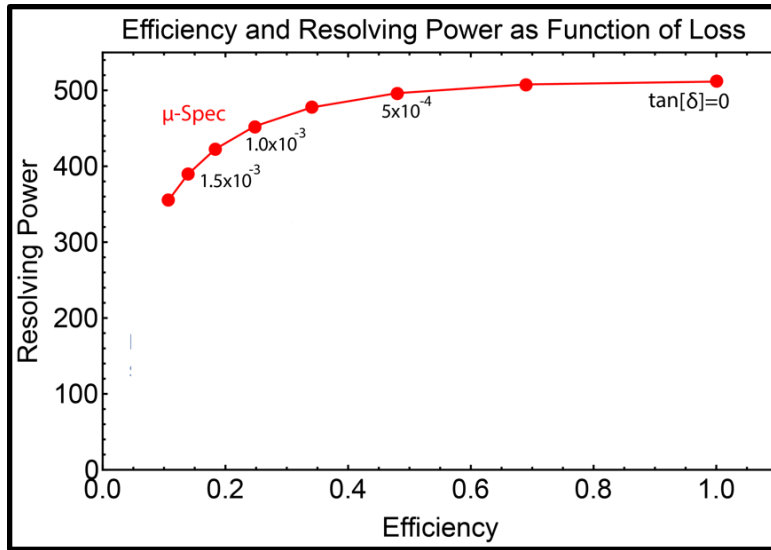## 3.4 Efficiency and Resolution Limits Due To Loss

Figure 3. μ-Spec efficiency and resolution as a function of loss for an $R = 500$ instrument. Here the loss tangent, $\tan \delta$, goes from 0 to 1.75×10^{-3} in steps of 2.5×10^{-4}.

The diffraction grating analog design of μ-Spec allows it to achieve unity efficiency in principle at its design resolution, with the ultimate limit to μ-Spec resolution and efficiency being set by the line loss of the material system. This dependence on loss from materials is illustrated in Fig. 3 where the resolving power and efficiency for a $R = 500$ design is plotted as a function of a material loss tangent. Here the effect of material loss on resolution and efficiency are determined by introducing an exponential loss term into a model of the delay network, where the resulting amplitudes at the emitter locations are reduced by the loss encountered over the given delay line lengths. A spectral function is then computed by taking the Fourier transform of this illuminated emitter pattern. We then extract the resulting resolution and efficiency by fitting Gaussians to these modeled spectral profiles. It should be noted that in this model the efficiency of coupling to the receivers is neglected and it has been assumed that all of the power incident on the focal plane is detected. It can be seen that the resolving power of the μ-Spec instrument is relatively insensitive to loss at low loss tangents.

We have chosen to implement single-crystal silicon which has more than an order of magnitude lower loss than deposited dielectrics (such as Si_3N_4). Single-crystal silicon has a loss tangent, $\tan \delta \approx 1 \times 10^{-5}$ [25–28] (and even better when loss reduction processes are applied[29–31]) which should allow up to $R \sim 1500$. It should be noted that for the diffraction grating analog design, the optimization of the instrument design is also insensitive to the precise loss value (it does not need to be known a priori).

4. MODIFICATIONS FROM R=64 TO HIGHER RESOLUTION DESIGNS

4.1 Higher Order Operation

There are a variety of schemes for scaling the μ-Spec design to higher resolutions. The simplest approach is to operate the spectrometer in a single order (as is the case for our $R = 64$ design) and allow the focal plane radius to scale linearly with the resolving power, where this radius is $\propto R/M$.[8] However in this case, the simplicity of the design is countered by the larger size of the device (see Sec 4.3). The spectrometer can be kept compact if it is operated in higher orders. In this version of the design different orders will overlap at the same receiving locations on the focal plane. Therefore, broadband order-sorting filters are inserted at the output of each receiver to separate the orders before each is sent to an individual detector. Note that in cases when the spectrometer is operated in higher orders, a given submillimeter frequency may have significant power which falls into two observed orders, but this power can be collected by detectors from both orders, without suffering a loss in efficiency.

We have designed and demonstrated a compact, superconducting bandpass filter suitable for this purpose, which operates from 285 to 650 GHz and with 13% fractional bandwidth per channel (manuscript in preparation). This filter concept is inspired by the mammalian cochlea,[33] which is a channelizing filter that covers three decades of bandwidth and 3,000 channels in a very small physical space. For implementation in a higher order design multiple order-sorting filter designs would be used by tuning parameters in the filter model such that each design receives the corresponding frequency near the center of the frequency band.

4.2 Detector Sensitivity

Table 1. KID specifications for a μ-Spec instrument on a balloon-borne platform. Our laboratory demonstration KID design is also shown for comparison.

	"Laboratory" Design	$R = 256$ Design ("Warm" Balloon)	$R = 512$ Design ("Cold" Balloon)
Optical Loading	$100 - 20$ pW	30 fW	50 aW
Readout Power	$100 - 20$ pW	30 fW	50 aW
HEMT Noise Temp.	5 K	5 K	5 K
Aluminum Thickness	100 nm	20 nm	10 nm
Q_{int} under loading	20,000-137,000	300,000	800,000
Readout Frequency	2.1-2.5 GHz	2.8-3.1 GHz	2.8-3.1 GHz
Detector NEP	$1.5 \times 10^{-15} - 5.5 \times 10^{-17}\ W/Hz^{1/2}$	$8 \times 10^{-18}\ W/Hz^{1/2}$	$3.5 \times 10^{-19}\ W/Hz^{1/2}$
BLIP NEP	$9 \times 10^{-16} - 4 \times 10^{-17}\ W/Hz^{1/2}$	$5 \times 10^{-18}\ W/Hz^{1/2}$	$2 \times 10^{-19}\ W/Hz^{1/2}$

For our $R = 64$ demonstration[4,6] we developed a "laboratory" KID design (see Table 1), which is well suited for testing with an external submillimeter source with power ~ 1 nW, as well as with a cryogenic blackbody source with power ~ 20 pW. This KID consisted of a half-wave superconducting transmission line resonator made of an aluminum film. We have chosen aluminum due to its low microwave loss and because its superconducting properties are well-understood.[34,35] We will use this same design for our planned laboratory demonstration of the $R = 256$ spectrometer. However, for a balloon-borne and ultimately space-borne instrument greater sensitivity is required. We have developed two new versions of this design with sensitivities suitable for a balloon flight instrument, also shown in Table 1. This more sensitive design is nearly identical to our laboratory design but makes use of aluminum film of reduced thickness to provide the increase in sensitivity. Critical to the performance of these designs is achieving thin aluminum films with high internal quality factors, Q_{int} $\sim$300,000 - 800,000. We plan to produce simple optically-coupled test devices with this design to achieve noise equivalent power, NEP$\sim 3 \times 10^{-19}\ W/Hz^{1/2}$ as required for balloon operation of μ-Spec. It should be noted that this sensitivity has already been demonstrated by Ref. 34 for aluminum KID designs.

4.3 Instrument Size

The area of a conventional spectrograph is the product of the length, set by the required amount of phase delay, and the width, set by the number of detectors, giving a limiting area of approximately $(N\lambda)^2$, which is about 1 m^2 for a resolving power ~ 1000 at $\lambda \sim 1$ mm. μ-Spec reduces the area of a high-resolution spectrometer (and also mass and volume) by orders of magnitude by using the advantages of superconducting microstrip technology with a single crystal silicon dielectric.

In the case that only a single order is used the focal plane radius scales linearly with resolution in order to accommodate the required sampling along the focal plane arc. The Rowland circle radius is ~ 12 mm for our $R = 64$ design and the full spectrometer chip size is 4.2 cm $\times$ 1.8 cm. With this low resolution design we can fit six instruments per each four-inch wafer. Scaling from this $R = 64$ design to $R = 256$, $R = 500$, and $R = 1500$ respectively, the Rowland circle radius becomes 48 mm, 94 mm and 27 cm operating at a single order. With a four-inch (or even six-inch) wafer size, it therefore becomes necessary to operate in higher orders to keep the device more compact.

In the case that the focal plane radius is fixed and the spectrometer is operated in multiple orders, the increase in size when scaling to higher resolutions is dominated by the increase in the footprints of the delay network and order-sorting filters and detectors. For the $R = 256$ design (details of this design are reported in Sec. 5), which operates in multiple orders, the resulting chip size is $\sim$5 cm $\times$ 3 cm. For this design four spectrometer chips will fit on a single four-inch wafer.
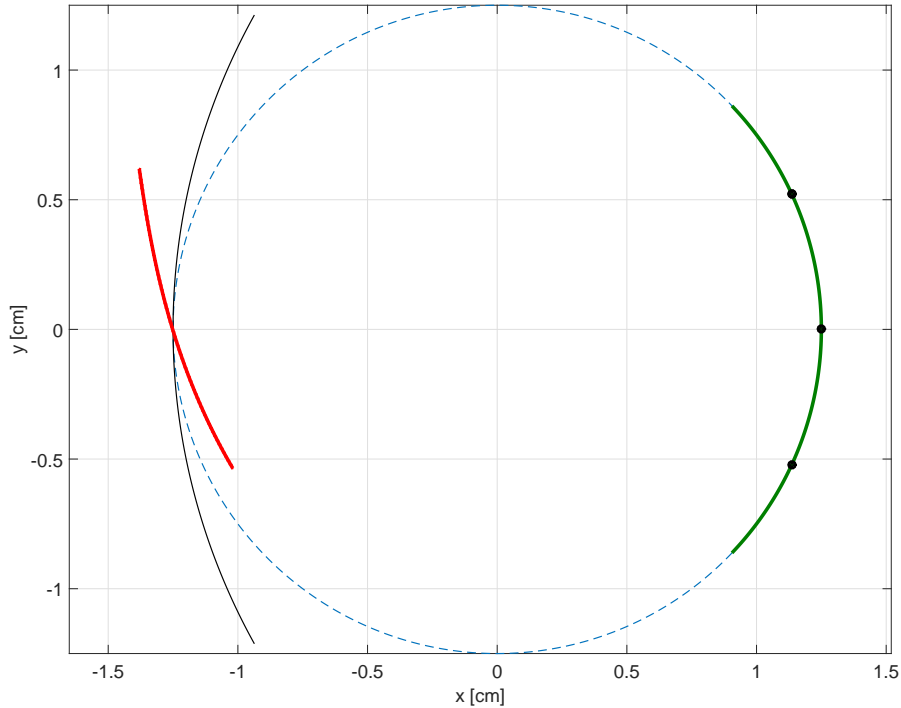

Figure 4. Physical layout of the 2-D parallel plate waveguide region design for a $R = 256$ μ-Spec. The emitter array, made of $N = 64$ feed antennas, is shown in red; the receiver array, made of 123 antennas, is shown in green. The dashed blue lines define the Rowland circle, upon which the receiving antennas are laid. The black line represents the grating of an ideal Rowland spectrometer. The $R = 256$ design differs from this ideal Rowland spectrometer because three stigmatic points (shown by the black dots) were imposed in optimization of the focal plane design.[8]

5. A DESIGN FOR $R=256$

We are in the process of finalizing the design for a $R = 256$ μ-Spec which we are developing for laboratory demonstration, and which is targeted for an eventual balloon-borne science instrument, when integrated with sensitive KID detectors (see Sec. 4.2). In Fig. 4 we show the focal plane layout for this $R = 256$ design, which was optimized following the procedures described in Ref. 8.
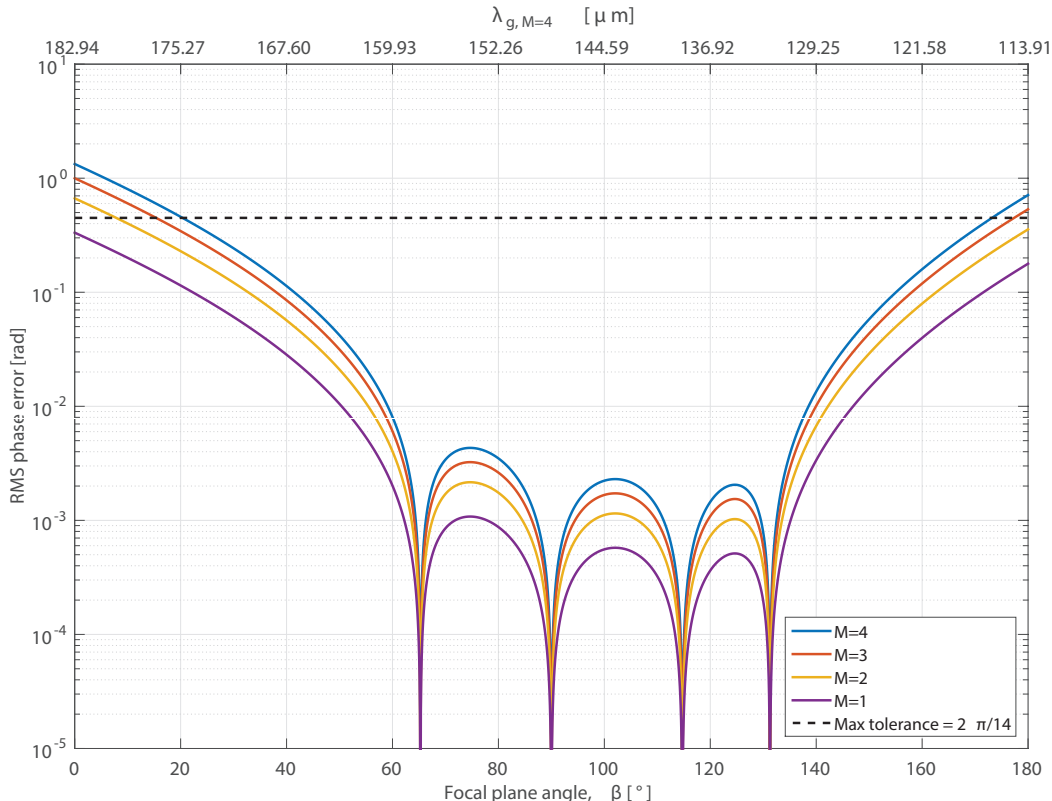

Figure 5. The RMS phase error is shown as a function of the focal plane angle, β, and the corresponding guide wavelengths, $\lambda_{g,M=4}$, on the focal plane for $M = 4$. The guide wavelengths for orders $M = 3$, 2 and 1 can be derived by multiplying $\lambda_{g,M=4}$ by 4/3, 2 and 4, respectively. Note the presence of a fourth unconstrained stigmatic point at $\beta \approx 132°$. The RMS phase error remains below the maximum allowed tolerance of $2\pi/14$ over more than $150°$. In our planned laboratory demonstration we will only be operating with orders $M = 2 - 4$, corresponding to operation between $\sim 350 - 650$ GHz

This design will operate in three orders ($M = 2 - 4$) with $N = 64$ emitters, and 123 receivers sampling the focal plane and with ~ 369 KIDs. This design will operate between $\sim 350 - 650$ GHz, which as discussed in Sec. 3.2 is near the bandwidth limits of the instrument elements with our current submillimeter design. In Fig. 5 the RMS phase error of the imaging across the focal is shown for the multiple orders of the design, demonstrating that our phase error criterion of $2\pi/14$ is satisfied (see also, Sec. 3.3.) In Fig. 6 the spectral response of five channels is shown, demonstrating the near-ideal $sinc^2$ function and the spectral purity of the design. Fig. 6 also shows that the the Nyquist sampling criterion is achieved. Here we have chosen sampling to match the Nyquist sampling criterion at the highest submillimeter frequency of 650 GHz.

6. CONCLUSIONS

We have presented an overview of the components and the design of the μ-Spec instrument, an integrated submillimeter spectrometer which is being developed for a balloon- or space-borne instrument. We have described a path towards realizing higher resolution versions of this instruments and the modifications required in extending
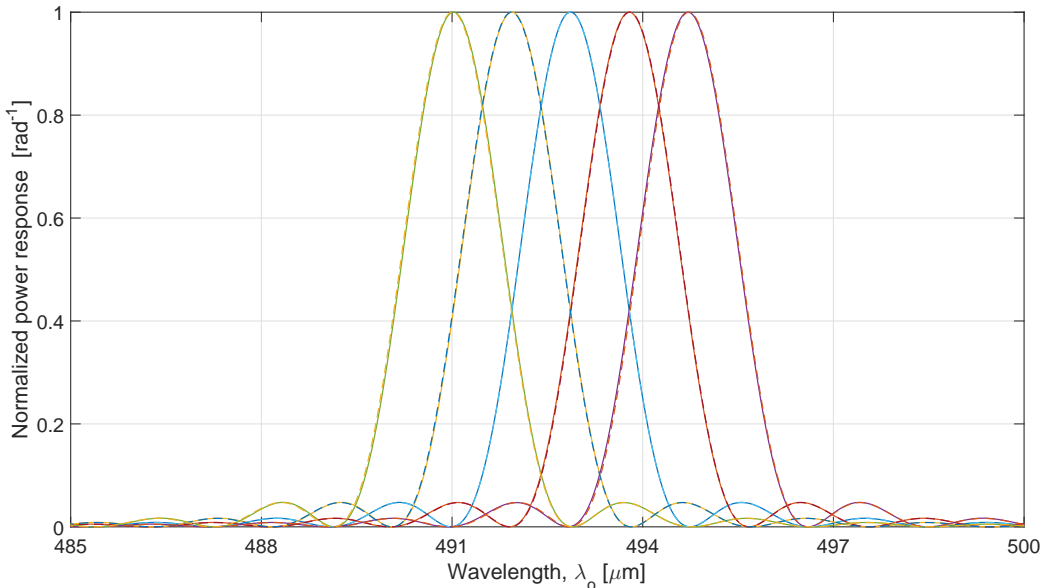
Figure 6. The angular power response for the $R = 256$ design. The emitter arrays angular power response (solid lines) is normalized by the total radiated power and plotted for five adjacent channels only (the full sampling of the design extends across the full wavelength band but is not shown in this plot). The dashed lines represent the ideal $sinc^2$ functions. One sees that the array response closely approximates this ideal function out to ~ 10 wavelengths. This $sinc$ function remains an approximation as the emitter array antennas are not uniformly illuminated.

this design from a $R = 64$ instrument which we have already demonstrated, to higher resolutions. Resolutions up to $R = 1500$ should be possible, with the instrument resolution limited only by material loss. A design limit that we are still currently exploring is the bandwidth for a single instrument. We also presented the details of our design for a $R = 256$ instrument, which we anticipate demonstrating in the laboratory within the next year, and which when integrated with sensitive detectors (see Sec. 4.2) could provide the first science results for μ-Spec, in a balloon-borne version of this instrument.

ACKNOWLEDGMENTS

REFERENCES

[1] Bradford, C., Goldsmith, P., Bolatto, A., Armus, L., Bauer, J., Appleton, P., Cooray, A., Casey, C., Dale, D., Uzgil, B., et al., "A cryogenic space telescope for far-infrared astrophysics: A vision for nasa in the 2020 decade," *arXiv preprint arXiv:1505.05551* (2015).

[2] Bradford, C. M., Ade, P. A., Aguirre, J. E., Bock, J. J., Dragovan, M., Duband, L., Earle, L., Glenn, J., Matsuhara, H., Naylor, B. J., et al., "Z-spec: a broadband millimeter-wave grating spectrometer: design, construction, and first cryogenic measurements," in [*SPIE Astronomical Telescopes+ Instrumentation*], 257–267, International Society for Optics and Photonics (2004).

[3] Armus, L., Bauer, J., Benford, D., Bergin, E., Bolatto, A., Bradford, C., Chen, C., Cooray, A., Evans, N., Farrah, D., Glenn, J., Goldsmith, P., Harris, A., Helou, G., Leisawitz, D., Lis, D., Marcum, P., Melnick, G., Milam, S., Mundy, L., Neufeld, D., Pontoppidan, K., Pope, A., Rizzo, M., Sandstrom, K., Sheth, K., and Wright, E., "From early galaxies to habitable planets: The science case and concept for a far-infrared surveyor," *2015 FIR Community Workshop Report* , 1–41 (2015).

9

[4] Noroozian, O., Barrentine, E., Brown, A., Cataldo, G., Ehsan, N., Hsieh, W.-T., Stevenson, T., U-yen, K., Wollack, E., and Moseley, S. H., "μ-spec: An efficient compact integrated spectrometer for submillimeter astrophysics," *26TH International Symposium on Space Terahertz Technology* (2015).

[5] Cataldo, G., Hsieh, W.-T., Huang, W.-C., Moseley, S. H., Stevenson, T. R., and Wollack, E. J., "Micro-spec: an ultracompact, high-sensitivity spectrometer for far-infrared and submillimeter astronomy," *Applied optics* **53**(6), 1094–1102 (2014).

[6] Barrentine, E. M., Noroozian, O., Brown, A. D., Cataldo, G., Ehsan, N., Hsieh, W.-T., Stevenson, T. R., U-Yen, K., Wollack, E. J., and Moseley, S. H., "Overview of the design, fabrication and performance requirements of micro-spec, an integrated submillimeter spectrometer," *16th International Workshop on Low Temperature Physisc* (2015).

[7] Rosen, D., Suzuki, A., Keating, B., Krantz, W., Lee, A. T., Quealy, E., Richards, P. L., Siritanasak, P., and Walker, W., "Epoxy-based broadband antireflection coating for millimeter-wave optics," *Applied optics* **52**(33), 8102–8105 (2013).

[8] Cataldo, G., Hseih, W.-T., Huang, W.-C., Moseley, S. H., Stevenson, T. R., and Wollack, E. J., "Micro-spec: an integrated direct-detection spectrometer for far-infrared space telescopes," *Proceedings SPIE* **9143**, 91432C–91432C–9 (2014).

[9] Archer, D., "Lens-fed multiple beam arrays," *Microwave Journal* **27**, 171 (1984).

[10] Rotman, W. and Turner, R. F., "Wide-angle microwave lens for line source applications," *Antennas and Propagation, IEEE Transactions on* **11**(6), 623–632 (1963).

[11] Naylor, B. J., *Broadband millimeter-wave spectroscopy with Z-Spec: an unbiased molecular-line survey of the starburst galaxy M82*, PhD thesis, California Institute of Technology (2008).

[12] Day, P. K., LeDuc, H. G., Mazin, B. A., Vayonakis, A., and Zmuidzinas, J., "A broadband superconducting detector suitable for use in large arrays," *Nature* **425**(6960), 817–821 (2003).

[13] Zmuidzinas, J., "Superconducting microresonators: physics and applications," *Annu. Rev. Condens. Matter Phys.* **3**(1), 169–214 (2012).

[14] McHugh, S., Mazin, B. A., Serfass, B., Meeker, S., OBrien, K., Duan, R., Raffanti, R., and Werthimer, D., "A readout for large arrays of microwave kinetic inductance detectors," *Review of Scientific Instruments* **83**(4), 044702 (2012).

[15] Mazin, B., Meeker, S., Strader, M., Szypryt, P., Marsden, D., van Eyken, J., Duggan, G., Walter, A., Ulbricht, G., Johnson, M., et al., "Arcons: a 2024 pixel optical through near-ir cryogenic imaging spectrophotometer," *Publications of the Astronomical Society of the Pacific* **125**(933), 1348 (2013).

[16] Wollack, E., Chuss, D., Rostem, K., and U-Yen, K., "Impedance matched absorptive thermal blocking filters," *Review of Scientific Instruments* **85**(3), 034702 (2014).

[17] U-yen, K. and Wollack, E. J., "Compact planar microwave blocking filter," in [*Microwave Conference, 2008. EuMC 2008. 38th European*], 642–645 (Oct 2008).

[18] Shirokoff, E., Barry, P. S., Bradford, C. M., Chattopadhyay, G., Day, P., Doyle, S., Hailey-Dunsheath, S., Hollister, M. I., Kovács, A., Leduc, H. G., McKenney, C. M., Mauskopf, P., Nguyen, H. T., O'Brient, R., Padin, S., Reck, T. J., Swenson, L. J., Tucker, C. E., and Zmuidzinas, J., "Design and performance of super-spec: An on-chip, kid-based, mm-wavelength spectrometer," *Journal of Low Temperature Physics* **176**(5), 657–662 (2014).

[19] Hailey-Dunsheath, S., Barry, P. S., Bradford, C. M., Chattopadhyay, G., Day, P., Doyle, S., Hollister, M., Kovacs, A., LeDuc, H. G., Llombart, N., Mauskopf, P., McKenney, C., Monroe, R., Nguyen, H. T., O'Brient, R., Padin, S., Reck, T., Shirokoff, E., Swenson, L., Tucker, C. E., and Zmuidzinas, J., "Optical measurements of superspec: A millimeter-wave on-chip spectrometer," *Journal of Low Temperature Physics* **176**(5), 841–847 (2014).

[20] Endo, A., Van der Werf, P., Janssen, R., De Visser, P., Klapwijk, T., Baselmans, J., Ferrari, L., Baryshev, A., and Yates, S., "Design of an integrated filterbank for deshima: On-chip submillimeter imaging spectrograph based on superconducting resonators," *Journal of Low Temperature Physics* **167**(3-4), 341–346 (2012).

[21] Endo, A., Sfiligoj, C., Yates, S., Baselmans, J., Thoen, D., Javadzadeh, S., van der Werf, P., Baryshev, A., and Klapwijk, T., "On-chip filter bank spectroscopy at 600–700 ghz using nbtin superconducting resonators," *Applied Physics Letters* **103**, 032601 (2013).

[22] Patel, A., Brown, A., Hsieh, W., Stevenson, T., Moseley, S. H., U-yen, K., Ehsan, N., Barrentine, E., Manos, G., and Wollack, E. J., "Fabrication of mkids for the microspec spectrometer," *Applied Superconductivity, IEEE Transactions on* **23**(3), 2400404–2400404 (2013).

[23] Brown, A. D. and Patel, A. A., "High precision metal thin film liftoff technique," (July 7 2015). US Patent 9,076,658.

[24] Bruel, M., Aspar, B., and Auberton-Herve, A.-J., "Smart-cut: a new silicon on insulator material technology based on hydrogen implantation and wafer bonding," *Japanese journal of applied physics* **36**(3S), 1636 (1997).

[25] Datta, R., Munson, C., Niemack, M., McMahon, J., Britton, J., Wollack, E. J., Beall, J., Devlin, M., Fowler, J., Gallardo, P., et al., "Large-aperture wide-bandwidth antireflection-coated silicon lenses for millimeter wavelengths," *Applied optics* **52**(36), 8747–8758 (2013).

[26] Duffar, T., [*Crystal growth processes based on capillarity: Czochralski, floating zone, shaping and crucible techniques*], John Wiley & Sons (2010).

[27] Krupka, J., Breeze, J., Centeno, A., Alford, N., Claussen, T., and Jensen, L., "Measurements of permittivity, dielectric loss tangent, and resistivity of float-zone silicon at microwave frequencies," *Microwave Theory and Techniques, IEEE Transactions on* **54**(11), 3995–4001 (2006).

[28] Afsar, M. N. and Chi, H., "Millimeter wave complex refractive index, complex dielectric permittivity and loss tangent of extra high purity and compensated silicon," *International Journal of Infrared and Millimeter Waves* **15**(7), 1181–1188 (1994).

[29] Afsar, M. N. and Chi, H., "Window materials for high power gyrotron," *International journal of infrared and millimeter waves* **15**(7), 1161–1179 (1994).

[30] Parshin, V., Heidinger, R., Andreev, B., Gusev, A., and Shmagin, V., "Silicon as an advanced window material for high power gyrotrons," *International journal of infrared and millimeter waves* **16**(5), 863–877 (1995).

[31] Molla, J., Vila, R., Heidinger, R., and Ibarra, A., "Radiation effects on dielectric losses of au-doped silicon," *Journal of nuclear materials* **258**, 1884–1888 (1998).

[32] Neto, A. and Lee, J., "Ultrawide-band properties of long slot arrays," *IEEE transactions on antennas and propagation* **54**(2), 534–543 (2006).

[33] Galbraith, C. J. and Rebeiz, G. M., "Higher order cochlea-like channelizing filters," *Microwave Theory and Techniques, IEEE Transactions on* **56**(7), 1675–1683 (2008).

[34] De Visser, P., Baselmans, J., Bueno, J., Llombart, N., and Klapwijk, T., "Fluctuations in the electron system of a superconductor exposed to a photon flux," *Nature communications* **5** (2014).

[35] Megrant, A., Neill, C., Barends, R., Chiaro, B., Chen, Y., Feigl, L., Kelly, J., Lucero, E., Mariantoni, M., OMalley, P., et al., "Planar superconducting resonators with internal quality factors above one million," *Applied Physics Letters* **100**(11), 113510 (2012).